JACS
JOURNAL OF THE AMERICAN CHEMICAL SOCIETY
Article
pubs.acs.org/JACS

Fluorescent Probe for Proton-Coupled DNA Folding Revealing Slow Exchange of *i*-Motif and Duplex Structures

Guillaume Mata and Nathan W. Luedtke*

Department of Chemistry, University of Zürich, Winterthurerstrasse 190, CH-8057 Zürich, Switzerland

Supporting Information

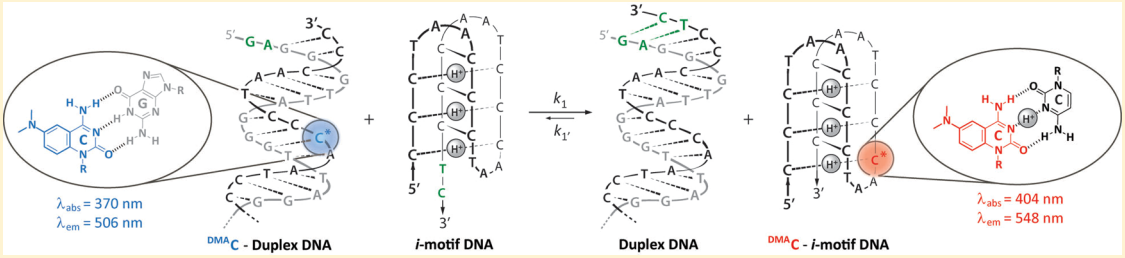

ABSTRACT: Ionized nucleobases participate in pairing interactions outside of Watson and Crick's rules. Base pairing and ionization can be coupled via global conformational changes to raise the apparent pK_a of protonated nucleobases to values above physiological pH. To provide the first specific reporter of proton-coupled DNA folding, we developed a "push−pull" fluorescent nucleoside analog composed of dimethylaniline (DMA) fused to deoxycytidine. "^{DMA}**C**" exhibits the same pK_a and base pairing characteristics as native cytosine residues in the human telomeric repeat sequence, where it causes little or no perturbation of DNA structure or stability. Upon protonation of ^{DMA}**C**, enhanced charge transfer results in large red shifting (+40 nm) of its excitation/emission maxima. ^{DMA}**C**'s fluorescence intensity, anisotropy, and energy transfer properties can be used to track conformational changes in real time. Strand displacement assays were conducted by mixing ^{DMA}**C**-labeled duplexes containing a 5′ single-stranded overhang with an excess of unlabeled DNA to initiate thermodynamically favorable unfolding−refolding reactions that release the ^{DMA}**C**-labeled strand from its complement. Rate constants for strand displacement upon addition of *i*-motif DNA (k = 1.0 M^{-1} s^{-1}, $t_{1/2}$ ≈ 12 h) were 320-fold lower than those measured upon addition of unfolded DNA (k = 3.2 × 10^2 M^{-1} s^{-1}, $t_{1/2}$ ≈ 2 min). These results reveal that *i*-motif structures having only marginal thermodynamic stabilities (T_m < 40 °C) can still pose large kinetic barriers to duplex formation under near-physiological conditions of pH (5.75), temperature (25 °C), and salt (100 mM NaCl).

INTRODUCTION

Acid-loving bacteria can thrive in strongly acidic conditions (pH ≤ 2) by maintaining their intracellular pH in the range 4.6−6.5.[1] The nuclear pH of eukaryotic cells is typically 7.3,[2] at which the canonical nucleobases are essentially uncharged in solution.[3] Ionized nucleobases are nonetheless observed in certain DNA and RNA structures at a neutral pH,[4] where they can mediate complex biological functions such as translational frame shifting[4g] and acid−base catalysis.[4h]

Cytidine is the most intrinsically basic canonical nucleobase, with a pK_a = 4.5 for its conjugate acid (C^+) in water.[3] Long-range electrostatic interactions and hydrogen bonding interactions can raise the effective pK_a (pK) of C^+ residues by as much as five units in folded nucleic acids. For example, G−C base pairs in duplex DNA can spontaneously adopt a transient G−C^+ Hoogsteen base pair that exhibits an apparent pK ≈ 7.2,[5] and CG−C^+ triplets involving both Watson and Crick and Hoogsteen base pairing interactions can exhibit pK values as high as 9.5.[4f]

The pH-dependent folding of C-rich DNA into *i*-motif structures containing "intercalated" C−C^+ base pairs is a highly cooperative process, with complete folding transitions occurring over as little as 0.3 pH units.[6] Depending on the DNA sequence, the apparent pK values for C−C^+ base pairs in *i*-motif structures range from 5.5 to 7.2.[7] These values can be further increased by partial DNA dehydration and/or ligand binding of *i*-motif structures.[8] Although much is known about the thermodynamics of *i*-motif folding *in vitro*,[9] very little is known about the kinetics of folding pathways involving competition between *i*-motif and duplex structures.[10] This competition could impact the biological activities of transient *i*-motif structures proposed to form *in vivo*.[11] However, the unambiguous detection of *i*-motif folded structures, or any other nucleic acid structure containing C^+ in cells, remains elusive.

DNA sequences present in large copy numbers provide attractive opportunities for the direct detection of noncanonical base pairing interactions in cells.[12] We therefore selected the cytosine-rich human telomeric repeat sequence

Received: August 25, 2014
Revised: November 4, 2014
Accepted: November 25, 2014
Published: November 25, 2014

DOI: 10.1021/ja508741u
J. Am. Chem. Soc. 2015, 137, 699−707

($^{5'}$CCCTAA$^{3'}$)$_n$[13] for the development of a new fluorescent cytidine mimic "^{DMA}C" that reports cytosine ionization upon proton-coupled DNA folding. ^{DMA}C has little or no impact on the structure or stability of duplex or *i*-motif structures, where it exhibits the same ionization characteristics as native cytosine residues. We have used ^{DMA}C-modified DNA to probe the local environment and base-stacking interactions of C−C$^+$ base pairs in *i*-motif structures and in strand displacement experiments to track the interconversion of duplex and *i*-motif structures under constant conditions of pH, salt, and temperature. Interestingly, *i*-motif structures that exhibited only marginal thermodynamic stabilities ($T_m \approx 38$ °C) at pH = 5.75 still posed large kinetic barriers ($t_{1/2} \approx 12$ h) to duplex formation at 25 °C. These results suggest that energy-dependent processes would be needed to resolve *i*-motif structures on a reasonable time scale *in vivo*.

RESULTS

Probe Design. FRET analysis of end-labeled oligonucleotides is a common approach for studying *i*-motif folding *in vitro*,[14] but the addition of two large fluorophores to oligonucleotides can perturb DNA structures, stabilities, and folding pathways.[15] We therefore focused on nucleobase analogs as minimally disrupting probes of nucleic acid structures and dynamics.[16] Some nucleobase mimics have previously been incorporated into the loops of *i*-motifs,[17] but no probe has been directly incorporated into a C−C$^+$ base pair.

The new fluorescent nucleoside analog *N*,*N*-dimethylaniline-2′-deoxycytidine (^{DMA}C) is composed of a dimethylaniline unit fused to 2′-deoxycytidine (Figure 1). The resulting quinazoline

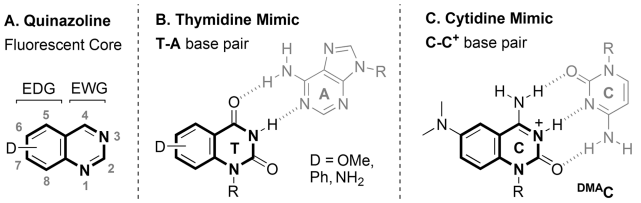

Figure 1. (A) Structure and numbering of quinazoline.[18] (B) Quinazoline-based thymidine mimic in Watson−Crick T−A base pair.[19] (C) Cytidine mimic ^{DMA}C in hemiprotonated C−C$^+$ base pair. R = deoxyribose.

core structure is already well recognized for its fluorescence properties[18] and for its ability to be well accommodated by duplexes.[19] Models based on high resolution structures[20] suggest that quinazoline-based cytidine mimics should cause no steric clashes in *i*-motif structures, even when further modified at position *C6* or *C7*. To facilitate sensitive reporting of *N3* protonation, an electron-donating dimethylamino group was included at the *C6* position. This position was selected because it is not in conjugation with *N3* and therefore expected to have little impact on its ground-state basicity. HOMO−LUMO calculations of ^{DMA}C suggest that a shift in electron density from dimethylaniline to cytosine upon photoexcitation would be enhanced upon protonation of *N3* (Figure 2). The calculated HOMO−LUMO gap for *N3*-protonated ^{DMA}C (ΔE = 2.86 eV) is lower than that of neutral ^{DMA}C (ΔE = 3.75 eV), thereby suggesting a red shift in fluorescence emission upon ^{DMA}C protonation at *N3*. In contrast, protonation at the *N6* dimethylamino group should result in a blue-shifted emission

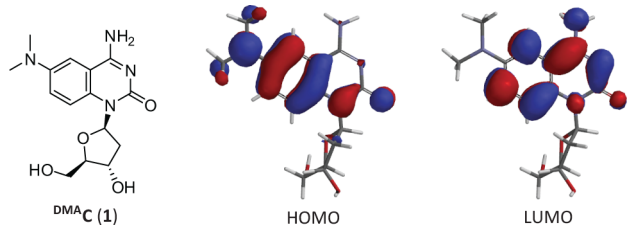

Figure 2. Structure of ^{DMA}C nucleoside (**1**) and molecular orbitals calculated from a DFT-optimized geometry using B3LYP/6-311++G**.

on the basis of its larger calculated HOMO−LUMO gap (ΔE = 4.27 eV, Figure S1, Supporting Information).

Synthesis of ^{DMA}C (1). Synthesis commenced from a previously reported 6-bromoquinazoline-2,4-(3*H*)-dione nucleoside **2** (Scheme 1).[21] Pd-catalyzed Buchwald−Hartwig amination of aryl halide **2** by Me_2NH was performed using a combination of $Pd_2(dba)_3$ and JohnPhos[22] to afford nucleoside **3** in 82% yield. To convert the resulting thymidine analog into a cytidine analog, **3** was treated with 2,4,6-triisopropylbenzenesulfonyl chloride (TPSCl) followed by aqueous ammonia. This two-step procedure afforded nucleoside **4** in 75% yield, which was deprotected with TBAF to give the ^{DMA}C nucleoside (**1**) in 91% isolated yield.

Scheme 1. Synthesis of ^{DMA}C Nucleoside (1)[a]

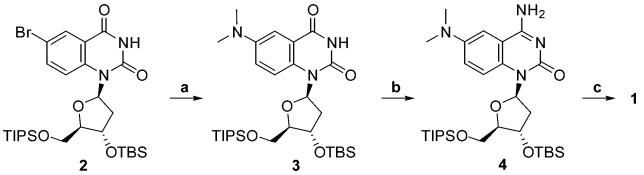

[a]Reaction conditions: (a) Me_2NH in THF (2.0 M), $Pd_2(dba)_3$ (5 mol %), JohnPhos (20 mol %), KOtBu, dioxane (0.15 M), 60 °C, 2 h, 82% yield. (b) (i) TPSCl, Et_3N, DMAP, CH_2Cl_2, 23 °C, 12 h; (ii) NH_4OH aq, THF, 23 °C, 10 min, 75% yield (over two steps). (c) TBAF, THF, 23 °C, 2 h, 91% yield. TIPS = triisopropylsilyl, TBS = *tert*-butyldimethylsilyl, JohnPhos = (biphenyl-2-yl)-di-*tert*-butyl-phosphane, TPSCl = 2,4,6-tri-isopropylbenzenesulfonyl chloride, DMAP = 4-dimethylaminopyridine, TBAF = tetra-*n*-butylammonium fluoride.

Conformation of ^{DMA}C Nucleoside (1). ^{1}H−^{1}H ROESY spectra of **1** indicate that its glycosidic bond adopts an *anti*-conformation. Strong cross-peaks between H8 and H2′β as well as H8 and H3′ were observed (Figure S2, Supporting Information). These are consistent with atomic distances obtained from a DFT energy-minimized *anti*-conformation (H8−H2′β = 2.39 Å and H8−H3′ = 2.90 Å, Table S3, Supporting Information). Additional ^{1}H−^{1}H ROESY correlations between H1′−H2′α and H1′−H4 indicate a β-configuration at *C1*. The ^{DMA}C nucleoside therefore possesses the same stereochemistry and conformational preferences as native deoxycytidine.

Photophysical Properties of ^{DMA}C Nucleoside (1). The maximal absorbance wavelengths of **1** (λ_{abs} = 365−425 nm, Table 1) are more than 100 nm to the red of DNA, thereby facilitating its selective excitation. Depending on the solvent polarity and acidity, nucleoside **1** exhibits highly variable quantum yields (Φ = 0.03−0.36) and maximal wavelengths of fluorescence emission (λ_{em} = 462−526 nm). To systematically characterize the environmental sensitivity of ^{DMA}C, absorption

DOI: 10.1021/ja508741u
J. Am. Chem. Soc. 2015, 137, 699−707

Table 1. Photophysical Properties of the ^{DMA}C Nucleoside (1)

solvent	λ_{abs} [a]	λ_{em} [b]	Stokes [c]	ε_{260} [d]	ε_{abs} [d]	Φ [e]
water	365	526	8.4	17.0	2.5	0.03
dioxane	390	462	4.0	20.0	2.9	0.36
MeCN	395	480	4.5	22.1	2.6	0.23
MeCN/HCl [f]	425	555	5.5	27.3	3.4	0.03

[a] λ_{abs} (nm) at the most red-shifted absorbance maxima. [b] λ_{em} in nm. [c] Stokes shifts in 10^3 cm^{-1}. [d] Extinction coefficients (ε) in 10^3 M^{-1} cm^{-1}. [e] Quinine hemisulfate (Φ = 0.55 at λ_{ex} = 370 nm)[25] in 0.5 M H_2SO_4 was used as a fluorescent standard for determining the relative quantum yields (Φ) of ^{DMA}C. [f] 1.0 equiv of anhydrous HCl was included.

and emission spectra were measured in water/dioxane mixtures. By plotting Stokes' shifts against Reichardt's solvent polarity parameter (E_T[30], Tables S4–S6, Supporting Information), we observed a linear slope of 166 cm^{-1}/(kcal mol^{-1}) (R^2 = 0.987).[23] This large slope validates ^{DMA}C as being a push–pull fluorophore.[24]

Protonation of ^{DMA}C (1). As a simple mimic of nucleobase environment,[26] acetonitrile was used as a solvent for characterizing the protonation-dependent photophysical properties of **1** (Table 1). Upon the addition of 1.0 equiv of HCl, ^{DMA}C exhibited pronounced red shifting of its absorbance (λ_{abs} = 395 → 425 nm) and emission wavelengths (λ_{em} = 485 → 555 nm, Figure 3). The addition of excess HCl resulted in dramatic blue shifting (λ_{abs} = 425 → 325 nm, and λ_{em} = 555 → 425 nm, Figure S7, Supporting Information). Taken together with the results of our HOMO–LUMO calculations, these results suggest that *N*3 is the primary protonation site of ^{DMA}C.

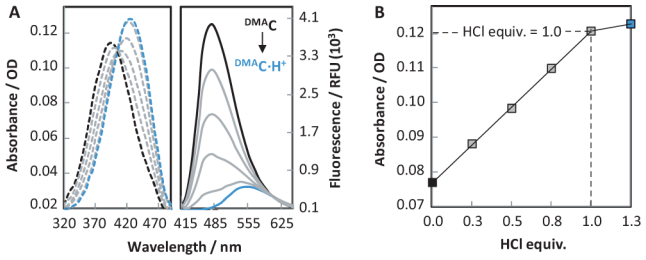

Figure 3. (A) Absorbance (---) and emission (—) spectra (λ_{ex} = 405 nm) of 40 μM ^{DMA}C (black) and ^{DMA}C·H$^+$ (blue) in MeCN upon addition of HCl. (B) Plot of absorbance intensity at λ_{abs} = 425 nm versus HCl equivalents added. See Figure S7 (Supporting Information) for spectra measured in the presence of excess HCl.

To measure the pK_a of protonated ^{DMA}C in water, its absorbance and emission spectra were evaluated as a function of pH (Figure 4A). The sigmoidal dependence of ^{DMA}C absorbance at 360 nm versus pH fit well to the Henderson–Hasselbalch equation for pK_a = 4.5 (Figure 4B). This is the same pK_a value as native cytidine.[3] Absorbance changes also revealed the emergence of absorbance over 440–480 nm with decreasing pH (Figure 4A), suggesting that ^{DMA}C might be used as a "turn-on" fluorescent probe for *i*-motif formation when selectively excited in this wavelength range.

Synthesis of ^{DMA}C-Modified DNA. To facilitate the site-specific incorporation of ^{DMA}C into DNA, synthesis of phosphoramidite **7** commenced with acetylation of nucleoside **4** to give **5** in 83% yield (Scheme 2). Following silyl group removal, DMT protection of the 5′-hydroxyl group furnished **6**

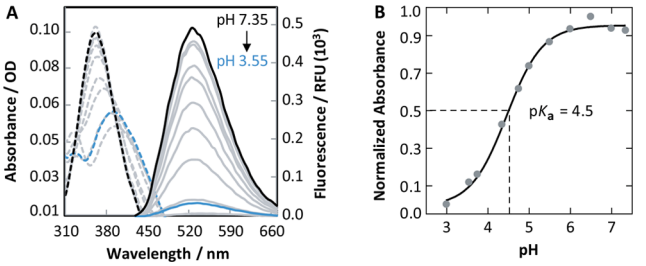

Figure 4. (A) Absorbance (---) and emission (—) spectra (λ_{ex} = 392 nm) of 40 μM ^{DMA}C (black) and ^{DMA}C·H$^+$ (blue) in phosphate citric acid buffer (200 mM Na_2HPO_4, 100 mM citric acid and 100 mM NaCl). (B) Plot of absorbance intensity at λ_{abs} = 360 nm versus pH. Similar results were obtained when analyzing the pH-dependent fluorescence changes (Figure S8, Supporting Information).

in a yield of 56% over two steps. Phosphitylation of the 3′-hydroxyl group gave **7** in an isolated yield of 71%. Phosphoramidite **7** was compatible with standard, automated DNA synthesis, although some deamination to give DNA containing the corresponding thymidine analog was observed as a minor side product. This could be removed by HPLC to give pure ^{DMA}C-modified oligonucleotides (Tables S9–S11, Supporting Information).

Scheme 2. Synthesis of ^{DMA}C Phosphoramidite (7)[a]

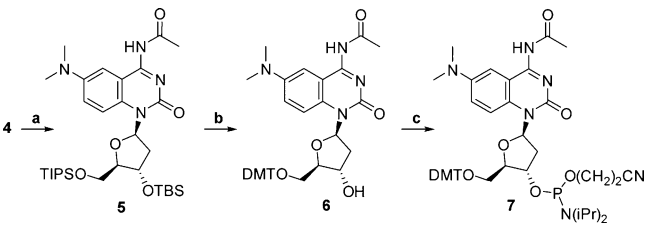

[a] Reaction conditions: (a) Ac_2O (1.2 equiv), DMAP (10 mol %), pyridine, 23 °C, 1 h, 83% yield. (b) (i) TBAF, THF, 23 °C, 2 h; (ii) DMT-Cl (1.2 equiv), pyridine, 23 °C, 45 min, 56% yield (over two steps). (c) 2-Cyanoethyl-*N*,*N*-diisopropylchloro-phosphoramidite (2.0 equiv), DIPEA, CH_2Cl_2, 0 °C, 45 min, 71% yield. TIPS = triisopropylsilyl, TBS = *tert*-butyldimethylsilyl, DMAP = 4-dimethylaminopyridine, DMT-Cl = 4,4′-dimethoxytrityl chloride, DIPEA = *N*,*N*-diisopropylethylamine, TBAF = tetra-*n*-butylammonium fluoride.

Under acidic conditions, the cytosine-rich human telomeric repeat sequence ($^{5'}$CCCTAA$^{3'}$)$_4$ folds into two closely related *i*-motif conformations *in vitro*, each containing six C–C$^+$ base pairs and three TAA loops (Figure 5).[13] ^{DMA}C was incorporated at single positions stacked between two other C–C$^+$ base pairs **TeloX2** and **TeloX14**, or at positions proximal to the loops **TeloX13** and **TeloX15** where **X** = ^{DMA}C.

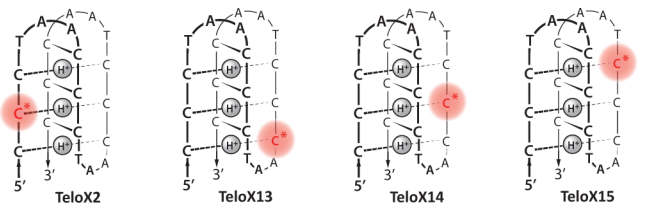

Figure 5. Secondary structure of a human telomeric *i*-motif containing the ^{DMA}C probe at four different positions. The dominant *i*-motif conformation "5′E" is shown.[13]

DOI: 10.1021/ja508741u
J. Am. Chem. Soc. 2015, 137, 699–707

Impact of ^{DMA}C on DNA Structure. Circular dichroism (CD) and thermal denaturation studies were used to evaluate the impact of ^{DMA}C on the global structure and stability of duplex and *i*-motif DNA. Oligonucleotides containing **X** = C (wild type), ^{DMA}C, T, or A at each site of incorporation (**X2**, **X13**, **X14**, and **X15**) were folded into *i*-motifs by heating and cooling single-stranded oligonucleotides in aqueous buffer at

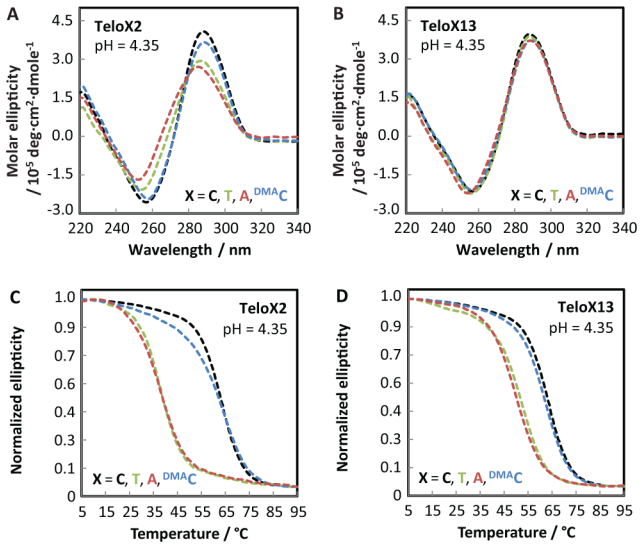

Figure 6. CD spectra at 25 °C of *i*-motif DNA: (A) **TeloX2** and (B) **TeloX13** with **X** = C (black), T (green), A (red) and ^{DMA}C (blue) at pH = 4.35. Thermal denaturation spectra (λ = 288 nm) of *i*-motif DNA of (C) **TeloX2** and (D) **TeloX13**. See Figures S12–S14, Supporting Information, for **TeloX14**, **TeloX15**, and duplex data.

pH = 4.35 or 5.50. The resulting CD spectra exhibited maxima at λ_{max} = 288 nm, minima at λ_{min} = 256 nm, and cooperative unfolding upon heating that are characteristic features of *i*-motif structures (Figure 6).[27] ^{DMA}C caused little, if any, impact on the global structure or stability of *i*-motifs as compared to that of the wild-type (wt) sequence containing cytosine (ΔT_m = +0.4 to −2.8 °C, Table 2). In contrast, mutant constructs containing A or T were dramatically destabilized (ΔT_m = −7.1 to −26.0 °C, Table 2). These results demonstrate that *i*-motif structures are exquisitely sensitive to base pair mismatches, and that ^{DMA}C is an excellent mimic of cytidine in this highly demanding context. This conclusion is further supported by pH-dependent *i*-motif folding experiments (Figure 7).

Duplex DNA structures were prepared by heating and cooling each oligonucleotide in aqueous buffer (pH = 7.35) in the presence of 1.1 equiv of complement strand. The CD spectra of the resulting duplexes exhibit characteristic maxima at λ_{max} = 264 nm, and minima at λ_{min} = 240 nm (Figure S14, Supporting Information).[27,28] ^{DMA}C caused little, if any, perturbation to the global structure or thermal stability of duplex DNA as compared to that of the wild type (ΔT_m = +1.4 to −0.8 °C, Table 2). In contrast, mutant constructs containing A–G and T–G mismatches exhibited significant thermal destabilizations as compared to that of the wild type (ΔT_m = −1.8 to −8.2 °C, Table 2). Taken together, these results demonstrate that ^{DMA}C is an excellent mimic of cytidine in both duplex and *i*-motif structures. To the best of our knowledge, ^{DMA}C is the first probe to be directly incorporated into C–C$^+$ and C–G base pairs without perturbing their structure or stability.

Table 2. Thermal Denaturation Melting Temperatures (T_m, °C)[a]

sequence	X	T_m *i*-motif at pH = 4.35	T_m *i*-motif at pH = 5.50	T_m duplex at pH = 7.35
Telo (wt)	C	62.6	38.5	64.9
TeloX2	T	38.3 (−24.3)	27.6 (−10.9)	63.1 (−1.8)
TeloX2	A	37.8 (−24.5)	25.3 (−13.2)	61.1 (−3.8)
TeloX2	^{DMA}C	61.7 (−0.9)	38.9 (+0.4)	64.5 (−0.4)
TeloX13	T	51.2 (−11.4)	31.4 (−7.1)	57.3 (−7.6)
TeloX13	A	49.6 (−13.0)	29.6 (−8.9)	58.3 (−6.6)
TeloX13	^{DMA}C	61.2 (−1.4)	37.6 (−0.9)	64.1 (−0.8)
TeloX14	T	38.7 (−23.9)	28.1 (−10.4)	56.9 (−8.0)
TeloX14	A	36.6 (−26.0)	27.8 (−10.7)	58.8 (−6.1)
TeloX14	^{DMA}C	61.6 (−1.0)	38.7 (+0.2)	65.9 (+1.0)
TeloX15	T	46.7 (−15.0)	28.5 (−10.0)	56.7 (−8.2)
TeloX15	A	45.5 (−17.1)	27.5 (−11.0)	57.5 (−7.4)
TeloX15	^{DMA}C	59.8 (−2.8)	36.9 (−1.6)	66.3 (+1.4)

[a]Values are given as T_m ($\pm\Delta T_m$) where ΔT_m is the deviation from the wild-type (wt) construct. All samples contained 5 μM DNA in a buffer containing 200 mM Na_2HPO_4, 100 mM citric acid, and 100 mM NaCl at pH = 4.35, pH = 5.50, or pH = 7.35. Reproducibility is within 0.3 °C of each reported value.

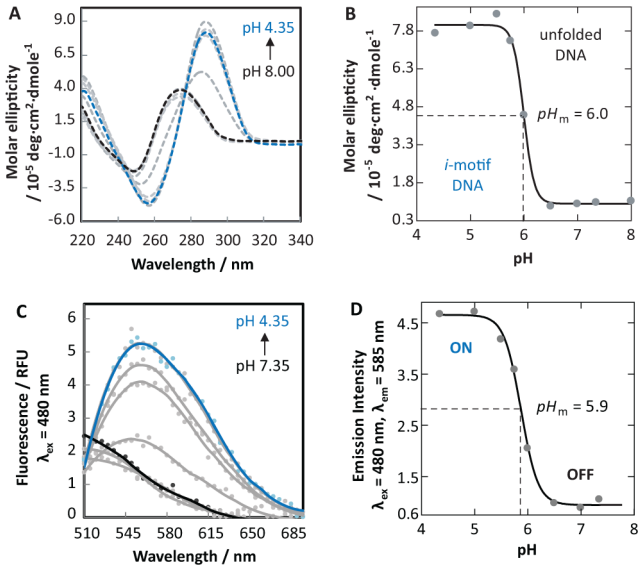

Figure 7. (A) CD spectra at 25 °C of **Telo** (wt) at pH = 4.35 (blue) and 8.00 (black) and at intermediate values (gray). (B) Plot of molar ellipticity (λ = 292 nm) versus pH. (C) Fluorescence spectra (λ_{ex} = 480 nm) of **TeloX13** (**X** = ^{DMA}C) at pH = 4.35–7.35. (D) Plot of fluorescence intensity (λ_{em} = 585 nm) versus pH. Samples contained 10 μM DNA in a buffer containing 200 mM Na_2HPO_4, 100 mM citric acid, and 100 mM NaCl.

pH-Dependent DNA Folding by CD and Fluorescence. CD and fluorescence spectroscopy were used to characterize the pH-dependent folding of single-stranded oligonucleotides into *i*-motif DNA.[27−29] At pH ≥ 6.50, the wild-type oligonucleotide exhibits a CD maximum at λ_{max} = 274 nm and minimum at λ_{min} = 249 nm, consistent with disordered states (Figure 7A).[27−29] When wild-type samples were heated and cooled at variable pH values, a transition from unfolded to

DOI: 10.1021/ja508741u
J. Am. Chem. Soc. 2015, 137, 699–707

i-motif structures was observed with a $^{1}/_{2}$ effective pH value (pH_m) of 6.0 (Figure 7B). All four of the ^{DMA}C-modified oligonucleotides also gave pH_m values = 6.0 ± 0.2 according to pH-dependent changes in fluorescence (Figure S15, Supporting Information). By selective excitation of protonated ^{DMA}C at 480 nm, a 5-fold increase in fluorescence emission upon *i*-motif folding was observed, with a pH_m value of 5.9 (Figure 7C,D). As for native cytosine residues, this value is 1.4 p*K* units higher than the pK_a value of ^{DMA}C in bulk solution (Figure 4).

Fluorescence Properties of ^{DMA}C in DNA. ^{DMA}C exhibits ca. 10-fold decreased quantum yields and ca. 35 nm red-shifted absorption and emission maxima in the context of *i*-motif versus unfolded DNA (Table 3). Consistent with *N3*

Table 3. Photophysical Data of ^{DMA}C in DNA (X = ^{DMA}C)

structure	sequence	λ_{abs} [a]	λ_{em} [b]	Φ [c]	η_t [d]	r [e]
unfolded	**TeloX2**	365	517	0.04	0.08	0.04
(pH = 7.35)	**TeloX13**	378	516	0.09	0.11	0.04
	TeloX14	365	520	0.06	0.06	0.04
	TeloX15	370	516	0.03	0.12	0.05
i-motif	**TeloX2**	400	542	0.004	0.12	0.24
(pH = 5.50)	**TeloX13**	405	551	0.01	0.15	0.17
	TeloX14	404	545	0.005	0.13	0.27
	TeloX15	407	548	0.006	0.17	0.21
duplex	**TeloX2**	365	512	0.02	0.05	0.15
(pH = 7.35)	**TeloX13**	365	505	0.11	0.04	0.14
	TeloX14	365	505	0.06	0.03	0.17
	TeloX15	365	502	0.04	0.08	0.16

[a] λ_{abs} (nm) are reported for the most red-shifted absorbance maxima. [b] λ_{em} in nm. [c] ^{DMA}C (**1**) was used as the fluorescent standard for the relative quantum yields (Φ) of ^{DMA}C in DNA. [d] DNA-to-probe energy transfer efficiencies (η_t) were calculated at λ_{ex} = 260 nm and at the maximum λ_{em} (see the Supporting Information for details). [e] Fluorescence anisotropy (r) calculated at pH = 7.35 (λ_{ex} = 370 nm, λ_{em} = 535 nm) or at pH = 5.50 (λ_{ex} = 410 nm, λ_{em} = 550 nm). All samples contained 4 μM DNA in an aqueous buffer (20 mM Na_2HPO_4, 10 mM citric acid, and 10 mM NaCl).

protonation upon *i*-motif folding, these changes closely resemble the ^{DMA}C nucleoside (**1**) upon its protonation in acetonitrile (Figure 2). The excitation spectra of ^{DMA}C-containing oligonucleotides exhibit two broad maxima centered at λ_{ex} ≈ 260 and 375 nm (Figure 8). The relatively large excitation peak at 260 nm of the ^{DMA}C-containing oligonucleotides as compared to that of the ^{DMA}C nucleoside (**1**) revealed the presence of energy transfer from unmodified bases to ^{DMA}C.[31] The corresponding energy transfer efficiencies (η_t) were much higher in *i*-motif structures (η_t = 0.17−0.12) than in the same oligonucleotides prepared as duplexes (η_t = 0.08−0.03, Table 3). These results are consistent with X-ray crystallographic analyses demonstrating that *i*-motifs have higher nucleobase densities and C−C$^+$ base pairs with unusually close base-stacking distances (3.1 Å) as compared to those of duplex DNA (3.4 Å).[20] Consistent with these observations, higher anisotropy values were observed for ^{DMA}C in the context of *i*-motif structures (r = 0.17−0.27) as compared to those of unfolded oligonucleotides (r = 0.04−0.05, Table 3), and intermediate values were observed for duplexes (Table 3). Given the larger hydrodynamic radius of duplex versus *i*-motif DNA,[32] these results suggest that local nucleobase dynamic motions are highly restricted in C−C$^+$ base

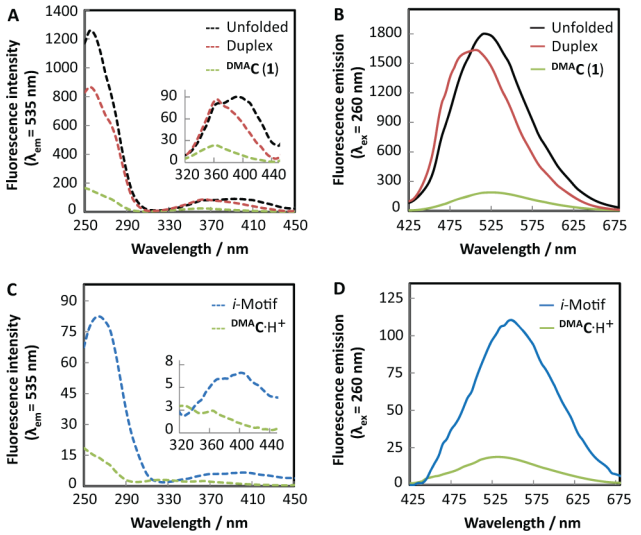

Figure 8. (A) Excitation (λ_{em} = 535 nm) and (B) emission (λ_{ex} = 260 nm) spectra of **TeloX13** (**X** = ^{DMA}C) at pH = 7.35.[30] (C) Excitation and (D) emission spectra at pH = 5.50. DNAs were prepared as unfolded (black), duplex (red), or *i*-motif (blue). Spectra of the ^{DMA}C nucleoside (pH = 7.35) and ^{DMA}C−**H**$^+$ (pH = 3.55) are shown in green. Sample conditions are given in Table 3. See Figure S17, Supporting Information for spectra collected from **TeloX2**, **TeloX14**, and **TeloX15**.

pairs. This conclusion is further supported by NMR proton−deuteron exchange experiments that demonstrated the protons in "internal" C−C$^+$ base pairs exchange very slowly (lifetime ≈ 1 h) with bulk solvent,[33] whereas exchange rates at sites neighboring loops are much faster (lifetime ≈ 1 ms).[33] Accordingly, the anisotropy values of ^{DMA}C were lower in C−C$^+$ base pairs proximal to loops (r = 0.17−0.21, **TeloX13** and **TeloX15**) than in "internal" C−C$^+$ base pairs of *i*-motifs (r = 0.24−0.27, **TeloX2** and **TeloX14**, Table 3).

In sum, the photophysical properties of ^{DMA}C provide well resolved and characteristic information about the folded state of the DNA containing it (Table 3). At all four sites of incorporation, ^{DMA}C emission maxima exhibited the following trends: *i*-motif (λ_{em} = 542−552 nm) > unfolded (λ_{em} = 516−520 nm) > duplex (λ_{em} = 502−512 nm). Fluorescence anisotropy values: *i*-motif (r = 0.17−0.27) > duplex (r = 0.14−0.17) > unfolded (r = 0.04−0.05). Energy transfer efficiencies: *i*-motif (η_t = 0.12−0.17) > unfolded (η_t = 0.06−0.12) > duplex (η_t = 0.03−0.08). By measuring multiple photophysical parameters of ^{DMA}C in parallel, we can therefore assign the structure of the DNA containing it.

Probing Real-Time DNA Dynamics with ^{DMA}C. Strand displacement assays were conducted to evaluate the ability of ^{DMA}C to serve as a real-time probe of DNA dynamics. In this approach, ^{DMA}C-containing oligonucleotides were prehybridized to a complementary sequence containing a variable-length "toehold" (TH) region to give a duplex "**GC**" containing a short, single-stranded overhang (Figure 9). Displacement of the ^{DMA}C-labeled strand was triggered upon addition of a 4-fold excess of an unlabeled invading strand "**I**" to produce a more stable duplex "**GI**" containing no single-stranded overhang. Displacement reactions were monitored using fluorescence anisotropy (Figure 10), and rate constants (k) were calculated using pseudo-first-order approximations as previously described.[34] The exact site of ^{DMA}C incorporation had very little (≤2-fold) impact on the measured k values (Table 4), but large

DOI: 10.1021/ja508741u
J. Am. Chem. Soc. 2015, 137, 699−707

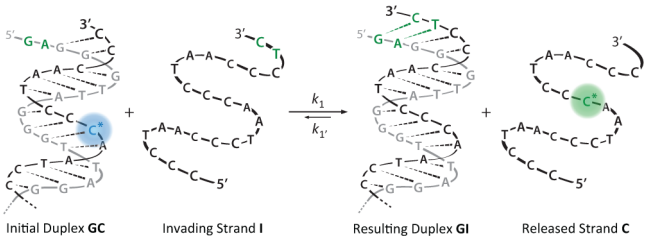

Figure 9. Representation of a "simple" strand displacement reaction at pH = 7.35 with **TeloX13** (X = ^{DMA}C) and a toehold of two nucleotides (green). See Table S18, Supporting Information for the oligonucleotide sequences used in strand displacement.

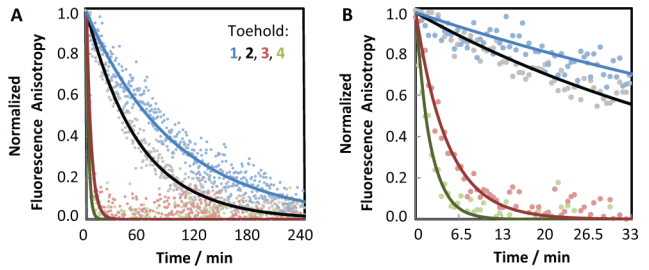

Figure 10. Real-time strand displacement according to fluorescence anisotropy (λ_{ex} = 370 nm, λ_{em} = 535 nm) of ^{DMA}C-modified oligonucleotide **TeloX13**. The lines represent the monoexponential fit of the data to eq 4. See Figure S20, Supporting Information, for data obtained using **TeloX2**, **TeloX14**, and **TeloX15**.

Table 4. Strand Displacement Rate Constants (k) in M^{-1} s^{-1} at pH = 7.35 for Different TH Lengths, Where X = ^{DMA}C[a]

sequence	TH = 1	TH = 2	TH = 3	TH = 4
TeloX2	1.8×10^1	3.4×10^1	3.1×10^2	6.1×10^2
TeloX13	1.1×10^1	1.8×10^1	2.1×10^2	4.6×10^2
TeloX14	1.0×10^1	1.8×10^1	1.7×10^2	4.2×10^2
TeloX15	0.9×10^1	1.3×10^1	1.7×10^2	2.7×10^2

[a]Rate constants k_1 were calculated by fitting fluorescence anisotropy to a single exponential decay eq 4 (see Materials and Methods). All reactions were conducted in an aqueous buffer containing 200 mM Na_2HPO_4, 100 mM citric acid, and 100 mM NaCl.

variations were observed with increasing TH lengths: $k_{TH1} = 1.1 \times 10^1 < k_{TH2} = 1.8 \times 10^1 < k_{TH3} = 2.1 \times 10^2 < k_{TH4} = 4.6 \times 10^2$ M^{-1} s^{-1} (Table 4). These rate constants are very similar to those previously reported using FRET-based constructs,[35] demonstrating that a single ^{DMA}C residue can replace the bulky end labels commonly used in FRET-based assays. Our results also demonstrate that the rate-limiting step of strand displacement is initiation rather than propagation, and that ^{DMA}C does not pose a significant barrier to either process.

***i*-Motif Structures Pose Large Kinetic Barriers to Duplex Formation.** To investigate the kinetic stability of *i*-motif structures according to their ability to inhibit duplex formation, we mixed an invading strand "**I**" with the ^{DMA}C-containing duplex "**GC**" under slightly acidic conditions (Figure 11). Strand displacement was monitored according to the fluorescence intensity changes at various pH values (Figure 12). At pH = 7.35, where the **I** strand is unstructured, nearly identical rate constants were obtained using fluorescence anisotropy (Table 4) and fluorescence intensity assays (Table 5). According to CD, the **I** strand exists as a 1:1 mixture of *i*-motif folded and unfolded DNA at pH = 6.0 (Figure 7A), yet

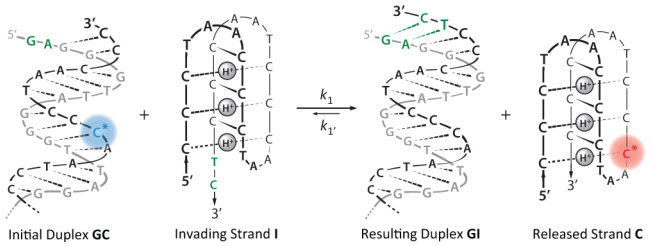

Figure 11. Representation of strand displacement reaction at pH ≤ 6.50 with **TeloX13** (X = ^{DMA}C) and a toehold of two nucleotides (green).

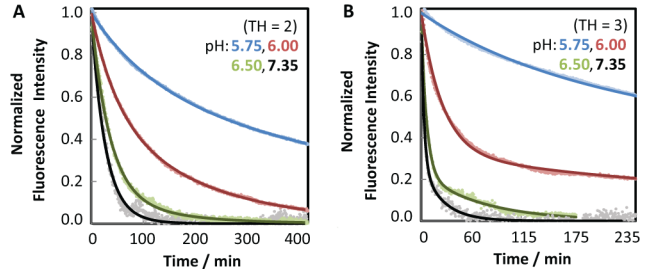

Figure 12. Strand displacement at pH = 7.35−5.75 according to the fluorescent intensity of **TeloX13** (X = ^{DMA}C) with toehold (A) TH = 2 and (B) TH = 3 (λ_{ex} = 370 nm and λ_{em} = 535 nm, 4 μM). Similar results were obtained for ^{DMA}C incorporated at **TeloX2** (Figure S23, Supporting Information). The points represent the measured fluorescence data and the lines represent the biexponential fitting to eq 5.

Table 5. Strand Displacement Rate Constants (k_1) in M^{-1} s^{-1} for Different pH Values and TH Lengths[a]

sequence	pH	TH = 2	TH = 3
TeloX13	7.35	4.1×10^1 (0.90)	3.2×10^2 (0.73)
X = ^{DMA}C	6.50	2.9×10^1 (0.87)	1.7×10^2 (0.77)
	6.00	0.54×10^1 (0.55)	4.1×10^1 (0.68)
	5.75	0.15×10^1 (0.66)	0.10×10^1 (0.68)

[a]Rate constants k_1 and k_2 were calculated from a biexponential fit of fluorescence intensity to eq 5. The dominant component (k_1) of each fit is reported, and its fractional contribution as compared to k_2 is given in parentheses. The minor components (k_2) were pH-independent, with values approximately equal to 1.8×10^1 M^{-1} s^{-1} (Tables S21 and S22, Supporting Information). These values are similar to those obtained by the "simple" strand displacement assay for TH = 2 (Table 4), suggesting that k_2 reflects strand displacement by a single-stranded, partially folded **I**.[38]

10-fold lower strand displacement rates were observed at pH = 6.0 than at pH = 7.35 (Figure 12 and Table 5). Given that a 4-fold excess of **I** strand was added, these results are consistent with previous studies that concluded *i*-motif folding is not a simple two-state process,[36] where all **I** strands possess at least some partial *i*-motif character at pH = 6.0 that lowers the rate of strand invasion. According to CD, the invading strand **I** is fully folded into an *i*-motif at pH = 5.75 (Figure 7A) that exhibits only marginal thermal stability (T_m = 31−38 °C, Figure S25 and Table S26, Supporting Information). The prefolded **GC** duplex, in contrast, exhibits high kinetic and thermodynamic stability over the entire pH range 5.75−7.35 (T_m = 61−65 °C, Figure S27, Supporting Information).[37] Upon mixing **GC** and **I** at pH = 5.75, the strand displacement rates were much lower than those observed at pH = 6.0 (Figure 12 and Table 5). In stark contrast to the results from the "simple" strand

DOI: 10.1021/ja508741u
J. Am. Chem. Soc. 2015, 137, 699−707

displacement experiments (Table 4), there was almost no difference in rate constants obtained for TH = 2 versus TH = 3 at pH = 5.75 (Table 5). These results strongly suggested that *i*-motif unfolding is the rate limiting step of strand displacement at pH = 5.75.

To evaluate the possibility that small differences in pH were responsible for slow strand displacement at pH 5.75−6.00 in an *i*-motif-independent way, a closely related invading strand mutant "$\mathbf{I_{mut}}$" was also evaluated (Table S19, Supporting Information). $\mathbf{I_{mut}}$ contains a central T−T base pair mismatch and is therefore incapable of forming a stable *i*-motif at pH = 5.75 and 25 °C (Figures S24 and S25, Supporting Information). Upon mixing ^{DMA}**C**-containing **GC** duplexes with $\mathbf{I_{mut}}$ oligonucleotides, little or no differences in rate constants were observed over the entire pH range 5.75−7.35, with values approximately equal to $k_{TH2} = 1.2 \times 10^2$ M^{-1} s^{-1} and $k_{TH3} = 5.8 \times 10^2$ M^{-1} s^{-1} (Table S28 and Figure S29, Supporting Information). Taken together, these results prove that the pH-dependent effects exhibited by the wild-type **I** are due to *i*-motif unfolding. A comparison of the rates measured at pH = 7.35 versus 5.75 (Table 5) reveals that *i*-motif unfolding presents a large kinetic barrier (320-fold difference for TH = 3) to duplex formation under near-physiological conditions of constant pH, temperature, and salt.

DISCUSSION AND CONCLUSIONS

Due to their relevance in biological and materials sciences, DNA structures containing noncanonical base pairs are rapidly gaining interest. Over the past decade, thermodynamically stable structures such as G-quadruplexes have received much attention,[12,39] whereas relatively little focus has been paid to their complementary DNA sequences that can fold into *i*-motif structures. One reason for this bias is that *i*-motif structures exhibit little or no thermodynamic stability at pH ≥ 7.2 in the absence of stabilizing factors.[8] The largest and most stable *i*-motif structures reported to date exhibit thermal denaturation temperatures of T_m = 27−32 °C at pH 7.0.[7b] Despite these low thermodynamic stabilities, mounting evidence suggests that *i*-motif structures may indeed possess biological functions. For example, a variety of natural proteins are known to selectively bind to and unfold *i*-motif structures.[40] As such, molecules that stabilize *i*-motif structures can potentially inhibit endogenous DNA unfolding pathways. Consistent with this type of activity, *i*-motif-stabilizing ligands have been shown to inhibit telomerase activity in cells[11a] and can trigger a transcriptional switch between two alternative folding pathways involving competition between hairpin and *i*-motif conformations.[11b,c] In the absence of stabilizing ligands, however, it is still unclear how endogenous *i*-motif structures, with such marginal thermodynamic stabilities, could impact gene regulation and/or chromosome stability. One possibility is that *i*-motif structures could impose kinetic, rather than thermodynamic, barriers to duplex formation.

Previous studies aimed at characterizing the kinetic parameters of *i*-motif/single-strand DNA transitions have utilized pH-jump experiments to trigger folding/unfolding.[13d,36b] These studies demonstrated that unimolecular *i*-motif folding occurs very rapidly ($t_{1/2} \approx 1$ s) at pH = 5.7, and unfolding is much slower ($t_{1/2} \approx 100$ s) at pH = 6.5.[36b] Although this approach provides a direct means to study folding kinetics, pH/temperature jumps initiate conformational changes of nucleic acids by perturbing the physical−chemical properties of the entire system. The resulting data can therefore not be interpolated to constant conditions of pH and temperature, where competition between alternative conformations would normally take place. In addition, C-rich DNA sequences, with few exceptions,[41] are found in the context of double-stranded DNA and therefore exist in complex equilibria involving duplex, G-quadruplex, and *i*-motif structures.[42] Most biologically relevant pathways are therefore expected to involve competition between inter- versus intramolecular folding pathways.[43]

To our knowledge, only a single previous study has attempted to quantify the kinetic barriers of duplex formation imposed by *i*-motif unfolding.[10] Sugimoto and co-workers used circular dichroism (CD) to evaluate duplex strand annealing rates upon mixing an *i*-motif with an "unfolded" single-stranded DNA under conditions of constant pH and temperature. Strand annealing at pH = 5.5 was approximately 10-fold slower than that measured at pH = 7.0. The authors concluded that *i*-motif unfolding was responsible, but residual DNA structure in the single-stranded G-rich DNA may have caused an underestimation of this effect.[44] Such residual structure is especially problematic in the case of G-rich strands, as it is extremely difficult in practice to eliminate all residual G-quadruplex-type structure.[45] The unfolding of the G-rich strands could have therefore been a major contributor to the rates measured at both pH values.

Strand displacement reactions are biologically relevant processes[46] that are compatible with the study of DNA (re)folding reactions under constant conditions of temperature, pH, and salt. We developed a novel strand displacement assay where the addition of excess unlabeled DNA is used to initiate a thermodynamically favorable unfolding−refolding reaction that displaces a ^{DMA}**C**-modified oligonucleotide from duplex DNA. This approach eliminates problems associated with residual G-quadruplex structure in the single-stranded G-rich DNA.[45] Given the negligible impact that ^{DMA}**C** has on DNA stability, the net thermodynamic driving force of *i*-motif unfolding, strand displacement, and refolding of the released strand "**C**" upon addition of an invading strand "**I**" is approximately the same for the unstructured **I** strand (Figure 9) as for the *i*-motif-folded **I** strand (Figure 10). At pH = 7.35, where the **I** strand is mostly unstructured, the kinetics of strand displacement are highly dependent on TH length (Table 4). In contrast, when the **I** strand is folded into an *i*-motif structure at pH = 5.75, the kinetics of strand displacement are independent of the TH length (Table 5). These results indicate that *i*-motif unfolding is the rate-limiting step for duplex formation under these conditions. The rate constants for strand displacement by *i*-motif DNA ($k = 1.0$ M^{-1} s^{-1}), were 320-fold lower than those measured for unfolded DNA ($k = 3.2 \times 10^2$ M^{-1} s^{-1}). These results are surprising, given the relatively low thermodynamic stabilities of the *i*-motif structures used here ($T_m \approx 38$ °C at pH = 5.75). Nucleic acid structures with only marginal thermodynamic stabilities can still pose large kinetic barriers ($t_{1/2} > 12$ h) to duplex formation. These results further suggest that the high mechanical stability of *i*-motif structures measured using optical tweezers is likely to be a kinetic rather than thermodynamic effect.[38] Together these results suggest that energy-dependent processes would be needed to resolve *i*-motif structures formed *in vivo*, especially in acid-loving bacteria where intracellular pH values can be found in the range 4.6−6.5.[1] The high kinetic stability of *i*-motif structures may provide a biological driving force for the evolution of *i*-motif-selective helicases and single-stranded DNA binding proteins that unfold *i*-motif structures.[40]

DOI: 10.1021/ja508741u
J. Am. Chem. Soc. 2015, 137, 699−707

The inhibition of *i*-motif unfolding could potentially lead to misregulation of certain biological processes *in vivo*, such as telomere capping,[11a] and gene regulation.[11b,c] Given the large kinetic barriers that *i*-motif structures can pose to strand displacement and duplex formation, small molecules that selectively inhibit the initiation and/or propagation of strand displacement could offer a novel therapeutic means to impact chromatin structure, function, and dynamics.

MATERIALS AND METHODS

^{DMA}**C**-modified duplexes containing **C** and **G** oligonucleotides (4 μM) were prepared in a phosphate citric acid buffer containing 200 mM Na_2HPO_4, 100 mM citric acid, and 100 mM NaCl (pH = 5.75−7.35). The invading strand **I** (4.0 equiv, final concentration 16 μM) was added at 25 °C, quickly mixed, and placed into the spectrometer to initiate the reaction. For the "simple" strand displacement assays conducted at pH = 7.35, the fluorescence anisotropy of the ^{DMA}**C**-modified oligonucleotide was measured at λ_{ex} = 370 nm and λ_{em} = 535 nm. For *i*-motif strand displacement assays, the fluorescence intensity was measured at λ_{ex} = 370 nm and λ_{em} = 535 nm. The strand displacement reaction can be modeled as a simple bimolecular reaction (eq 1) in which **GC** represents the initial duplex, **I** represents the incoming strand, **GI** represents the newly formed duplex, **C** represents the displaced ^{DMA}**C**-containing strand, and k_1 and $k_{1'}$ are the forward and backward rate constants:[34]

$$\mathbf{GC} + \mathbf{I} \underset{k_{1'}}{\overset{k_1}{\rightleftarrows}} \mathbf{GI} + \mathbf{C} \tag{1}$$

Given the higher kinetic and thermodynamic stability of **GI** versus **GC**, the back-reaction $k_{1'}$ is neglected. The strand displacement reaction can therefore be given as a function of time (t) (eq 2):

$$\frac{[\mathbf{C}]}{[\mathbf{GC}]_0} = \frac{k_1[\mathbf{I}]_0 t}{1 + k_1[\mathbf{I}]_0 t} \tag{2}$$

The concentration of the incoming strand ($[\mathbf{I}]_0$ = 16 μM) is much higher the initial duplex ($[\mathbf{GC}]_0$ = 4 μM). The time-dependent displacement reaction can therefore be approximated by (eq 3)

$$\frac{[\mathbf{C}]}{[\mathbf{GC}]_0} = 1 - e^{-k_1[\mathbf{I}]_0 t} \tag{3}$$

Accordingly, the "simple" strand displacement reactions were fit to the monoexponential equation (eq 4), where the rate constant k_1 is obtained by fitting the anisotropy (r) versus time (t):

$$r = e^{-k_1[\mathbf{I}]_0 t} \tag{4}$$

Strand displacement reactions involving *i*-motifs were fit to a biexponential equation (eq 5), where the rate constants k_1 and k_2 are obtained by fitting the fluorescence intensity (f) versus time (t) and where Fr is the fractional contribution:

$$f = \mathrm{Fr}_1 \cdot e^{-k_1[\mathbf{I}]_0 t} + \mathrm{Fr}_2 \cdot e^{-k_2[\mathbf{I}]_0 t} \tag{5}$$

ASSOCIATED CONTENT

Supporting Information

Description of materials and methods, oligonucleotide sequences, computational details, synthetic procedures and NMR spectra of isolated compounds, fluorescence spectra of ^{DMA}**C** nucleoside (**1**), additional circular dichroism (CD), thermal denaturation (T_m) and fluorescence spectra, fluorescence correction factors, energy transfer efficiencies, strand displacement data, HR-MS spectra, and HPLC traces of the ^{DMA}**C**-containing oligonucleotides. This material is available free of charge via the Internet at http://pubs.acs.org.

AUTHOR INFORMATION

Corresponding Author

nathan.luedtke@chem.uzh.ch

Notes

The authors declare no competing financial interest.

ACKNOWLEDGMENTS

The Swiss National Science Foundation (#146754) and the University of Zürich are gratefully acknowledged.

REFERENCES

(1) Baker-Austin, C.; Dopson, M. *Trends Microbiol.* **2007**, *15*, 165.

(2) Llopis, J.; McCaffery, J. M.; Miyawaki, A.; Farquhar, M. G.; Tsien, R. Y. *Proc. Natl. Acad. Sci. U. S. A.* **1998**, *95*, 6803.

(3) (a) Christensen, J. J.; Rytting, J. H.; Izatt, R. M. *J. Phys. Chem.* **1967**, *71*, 2700. (b) Izatt, R. M.; Christensen, J. J.; Rytting, J. H. *Chem. Rev.* **1971**, *71*, 439.

(4) (a) Robinson, H.; Wang, A. H. J. *Proc. Natl. Acad. Sci. U. S. A.* **1993**, *90*, 5224. (b) Volker, J.; Klump, H. H. *Biochemistry* **1994**, *33*, 13502. (c) Plum, G. E.; Breslauer, K. J. *J. Mol. Biol.* **1995**, *248*, 679. (d) Gaffney, B. L.; Kung, P. P.; Wang, C.; Jones, R. A. *J. Am. Chem. Soc.* **1995**, *117*, 12281. (e) Yu, A.; Barren, M. D.; Romero, R. M.; Christy, M.; Gold, B.; Dai, J. L.; Gray, D. M.; Haworth, I. S.; Mitas, M. *Biochemistry* **1997**, *36*, 3687. (f) Asensio, J. L.; Lane, A. N.; Dhesi, J.; Bergqvist, S.; Brown, T. *J. Mol. Biol.* **1998**, *275*, 811. (g) Nixon, P. L.; Giedroc, D. P. *J. Mol. Biol.* **2000**, *296*, 659. (h) Das, S. R.; Piccirilli, J. A. *Nat. Chem. Biol.* **2005**, *1*, 45.

(5) Nikolova, E. N.; Goh, G. B.; Brooks, C. L.; Al-Hashimi, H. M. *J. Am. Chem. Soc.* **2013**, *135*, 6766.

(6) (a) Gehring, K.; Leroy, J. L.; Gueron, M. *Nature* **1993**, *363*, 561. (b) Lieblein, A. L.; Kramer, M.; Dreuw, A.; Furtig, B.; Schwalbe, H. *Angew. Chem., Int. Ed.* **2012**, *51*, 4067. (c) Nesterova, I. V.; Nesterov, E. E. *J. Am. Chem. Soc.* **2014**, *136*, 8843.

(7) (a) Brooks, T. A.; Kendrick, S.; Hurley, L. *FEBS J.* **2010**, *277*, 3459. (b) Brazier, J. A.; Shah, A.; Brown, G. D. *Chem. Commun.* **2012**, *48*, 10739.

(8) (a) Li, X.; Peng, Y. H.; Ren, J. S.; Qu, X. G. *Proc. Natl. Acad. Sci. U. S. A.* **2006**, *103*, 19658. (b) Rajendran, A.; Nakano, S.; Sugimoto, N. *Chem. Commun.* **2010**, *46*, 1299. (c) Zhou, J.; Wei, C. Y.; Jia, G. Q.; Wang, X. L.; Feng, Z. C.; Li, C. *Mol. BioSyst.* **2010**, *6*, 580.

(9) (a) Benabou, S.; Aviñó, A.; Eritja, R.; González, C.; Gargallo, R. *RSC Adv.* **2014**, *4*, 26956. (b) Liu, D. S.; Balasubramanian, S. *Angew. Chem., Int. Ed.* **2003**, *42*, 5734.

(10) Li, W.; Miyoshi, D.; Nakano, S.; Sugimoto, N. *Biochemistry* **2003**, *42*, 11736.

(11) (a) Chen, Y.; Qu, K.; Zhao, C.; Wu, L.; Ren, J.; Wang, J.; Qu, X. *Nat. Commun.* **2012**, *3*, 1074. (b) Kendrick, S.; Kang, H. J.; Alam, M. P.; Madathil, M. M.; Agrawal, P.; Gokhale, V.; Yang, D. Z.; Hecht, S. M.; Hurley, L. H. *J. Am. Chem. Soc.* **2014**, *136*, 4161. (c) Kang, H. J.; Kendrick, S.; Hecht, S. M.; Hurley, L. H. *J. Am. Chem. Soc.* **2014**, *136*, 4172. (d) Cui, Y. X.; Koirala, D.; Kang, H.; Dhakal, S.; Yangyuoru, P.; Hurley, L. H.; Mao, H. B. *Nucleic Acids Res.* **2014**, *42*, 5755.

(12) (a) Schaffitzel, C.; Berger, I.; Postberg, J.; Hanes, J.; Lipps, H. J.; Pluckthun, A. *Proc. Natl. Acad. Sci. U. S. A.* **2001**, *98*, 8572. (b) Biffi, G.; Tannahill, D.; McCafferty, J.; Balasubramanian, S. *Nat. Chem.* **2013**, *5*, 182.

(13) (a) Phan, A. T.; Gueron, M.; Leroy, J. L. *J. Mol. Biol.* **2000**, *299*, 123. (b) Gueron, M.; Leroy, J. L. *Curr. Opin. Struct. Biol.* **2000**, *10*, 326.

DOI: 10.1021/ja508741u
J. Am. Chem. Soc. 2015, 137, 699−707

(c) Du, Z. H.; Yu, J. H.; Chen, Y. H.; Andino, R.; James, T. L. *J. Biol. Chem.* **2004**, *279*, 48126. (d) Lieblein, A. L.; Buck, J.; Schlepckow, K.; Furtig, B.; Schwalbe, H. *Angew. Chem., Int. Ed.* **2012**, *51*, 250.
(14) (a) Mergny, J. L. *Biochemistry* **1999**, *38*, 1573. (b) Choi, J.; Kim, S.; Tachikawa, T.; Fujitsuka, M.; Majima, T. *J. Am. Chem. Soc.* **2011**, *133*, 16146.
(15) (a) Mergny, J. L.; Maurizot, J. C. *ChemBioChem* **2001**, *2*, 124. (b) Moreira, B. G.; You, Y.; Behlke, M. A.; Owczarzy, R. *Biochem. Biophys. Res. Commun.* **2005**, *327*, 473.
(16) (a) Michel, J.; Gueguen, G.; Vercauteren, J.; Moreau, S. *Tetrahedron* **1997**, *53*, 8457. (b) Greco, N. J.; Tor, Y. *J. Am. Chem. Soc.* **2005**, *127*, 10784. (c) Srivatsan, S. G.; Greco, N. J.; Tor, Y. *Angew. Chem., Int. Ed.* **2008**, *47*, 6661. (d) Dumas, A.; Luedtke, N. W. *J. Am. Chem. Soc.* **2010**, *132*, 18004. (e) Sinkeldam, R. W.; Greco, N. J.; Tor, Y. *Chem. Rev.* **2010**, *110*, 2579. (f) Nadler, A.; Strohmeier, J.; Diederichsen, U. *Angew. Chem., Int. Ed.* **2011**, *50*, 5392. (g) Tanpure, A. A.; Pawar, M. G.; Srivatsan, S. G. *Isr. J. Chem.* **2013**, *53*, 366. (h) Sproviero, M.; Fadock, K. L.; Witham, A. A.; Manderville, R. A.; Sharma, P.; Wetmore, S. D. *Chem. Sci.* **2014**, *5*, 788. (i) Godde, F.; Toulme, J. J.; Moreau, S. *Nucleic Acids Res.* **2000**, *28*, 2977. (j) Liu, C. H.; Martin, C. T. *J. Mol. Biol.* **2001**, *308*, 465. (k) Sandin, P.; Wilhelmsson, L. M.; Lincoln, P.; Powers, V. E. C.; Brown, T.; Albinsson, B. *Nucleic Acids Res.* **2005**, *33*, 5019. (l) Miyata, K.; Tamamushi, R.; Ohkubo, A.; Taguchi, H.; Seio, K.; Santa, T.; Sekine, M. *Org. Lett.* **2006**, *8*, 1545. (m) Akiyama, Y.; Ma, Q.; Edgar, E.; Laikhter, A.; Hecht, S. M. *Org. Lett.* **2008**, *10*, 2127. (n) Greco, N. J.; Sinkeldam, R. W.; Tor, Y. *Org. Lett.* **2009**, *11*, 1115.
(17) (a) Hurley, L. H.; Kendrick, S.; Akiyama, Y.; Hecht, S. M. *J. Am. Chem. Soc.* **2009**, *131*, 17667. (b) Choi, J.; Tanaka, A.; Cho, D. W.; Fujitsuka, M.; Majima, T. *Angew. Chem.* **2013**, *52*, 12937. (c) Park, J. W.; Seo, Y. J.; Kim, B. H. *Chem. Commun.* **2014**, *50*, 52.
(18) (a) Liu, D.; Zhang, Z. Y.; Zhang, H. Y.; Wang, Y. *Chem. Commun.* **2013**, *49*, 10001. (b) Mata, G.; Luedtke, N. W. *Org. Lett.* **2013**, *15*, 2462. (c) Achelle, S.; Rodriguez-Lopez, J.; Robin-le Guen, F. *J. Org. Chem.* **2014**, *79*, 7564.
(19) (a) Xie, Y.; Dix, A. V.; Tor, Y. *J. Am. Chem. Soc.* **2009**, *131*, 17605. (b) Xie, Y.; Maxson, T.; Tor, Y. *Org. Biomol. Chem.* **2010**, *8*, 5053. (c) Xie, Y.; Maxson, T.; Tor, Y. *J. Am. Chem. Soc.* **2010**, *132*, 11896.
(20) (a) Kang, C. H.; Berger, I.; Lockshin, C.; Ratliff, R.; Moyzis, R.; Rich, A. *Proc. Natl. Acad. Sci. U. S. A.* **1994**, *91*, 11636. (b) Chen, L.; Cai, L.; Zhang, X.; Rich, A. *Biochemistry* **1994**, *33*, 13540.
(21) Mata, G.; Luedtke, N. W. *J. Org. Chem.* **2012**, *77*, 9006.
(22) Surry, D. S.; Buchwald, S. L. *Angew. Chem., Int. Ed.* **2008**, *47*, 6338.
(23) (a) Reichardt, C. *Chem. Rev.* **1994**, *94*, 2319. (b) Sinkeldam, R. W.; Tor, Y. *Org. Biomol. Chem.* **2007**, *5*, 2523.
(24) (a) Netzel, T. L.; Zhao, M.; Nafisi, K.; Headrick, J.; Sigman, M. S.; Eaton, B. E. *J. Am. Chem. Soc.* **1995**, *117*, 9119. (b) Butler, R. S.; Cohn, P.; Tenzel, P.; Abboud, K. A.; Castellano, R. K. *J. Am. Chem. Soc.* **2009**, *131*, 623.
(25) Melhuish, W. H. *J. Phys. Chem.* **1961**, *65*, 229.
(26) Sinkeldam, R. W.; Greco, N. J.; Tor, Y. *ChemBioChem* **2008**, *9*, 706.
(27) Kypr, J.; Kejnovska, I.; Renciuk, D.; Vorlickova, M. *Nucleic Acids Res.* **2009**, *37*, 1713.
(28) Gray, D. M.; Ratliff, R. L.; Vaughan, M. R. *Methods Enzymol.* **1992**, *211*, 389.
(29) Guo, K.; Gokhale, V.; Hurley, L. H.; Sun, D. *Nucleic Acids Res.* **2008**, *36*, 4598.
(30) Although the fluorescence emission spectra are shown with λ_{ex} = 260 nm, selective excitation of the probe at λ_{ex} = 365−405 nm was also performed to calculate the quantum yields of ^{DMA}C in DNA.
(31) (a) Vaya, I.; Gustavsson, T.; Miannay, F. A.; Douki, T.; Markovitsi, D. *J. Am. Chem. Soc.* **2010**, *132*, 11834. (b) Kelley, S. O.; Barton, J. K. *Science* **1999**, *283*, 375. (c) Xu, D. G.; Nordlund, T. M. *Biophys. J.* **2000**, *78*, 1042. (d) Nordlund, T. M. *Photochem. Photobiol.* **2007**, *83*, 625.
(32) Wu, S.; Wang, X. Y.; Ye, X. D.; Zhang, G. Z. *J. Phys. Chem. B* **2013**, *117*, 11541.
(33) Esmaili, N.; Leroy, J. L. *Nucleic Acids Res.* **2005**, *33*, 213.
(34) (a) Zhang, D. Y.; Winfree, E. *J. Am. Chem. Soc.* **2009**, *131*, 17303. (b) Genot, A. J.; Zhang, D. Y.; Bath, J.; Turberfield, A. J. *J. Am. Chem. Soc.* **2011**, *133*, 2177. (c) Tang, W.; Wang, H.; Wang, D.; Zhao, Y.; Li, N.; Liu, F. *J. Am. Chem. Soc.* **2013**, *135*, 13628.
(35) Zhang, D. Y.; Seelig, G. *Nat. Chem.* **2011**, *3*, 103.
(36) (a) Dettler, J. M.; Buscaglia, R.; Cui, J. J.; Cashman, D.; Blynn, M.; Lewis, E. A. *Biophys. J.* **2010**, *99*, 561. (b) Chen, C.; Li, M.; Xing, Y. Z.; Li, Y. M.; Joedecke, C. C.; Jin, J.; Yang, Z. Q.; Liu, D. S. *Langmuir* **2012**, *28*, 17743. (c) Dhakal, S.; Lafontaine, J. L.; Yu, Z. B.; Koirala, D.; Mao, H. B. *PLoS One* **2012**, *7*, e39271.
(37) Studies have shown that the stability of G−C and A−T Watson−Crick base pairs is pH-independent for pH = 2−10.[9a]
(38) Dhakal, S.; Schonhoft, J. D.; Koirala, D.; Yu, Z. B.; Basu, S.; Mao, H. B. *J. Am. Chem. Soc.* **2010**, *132*, 8991.
(39) (a) Lipps, H. J.; Rhodes, D. *Trends Cell Biol.* **2009**, *19*, 414. (b) Bochman, M. L.; Paeschke, K.; Zakian, V. A. *Nat. Rev. Genet.* **2012**, *13*, 770. (c) Vummidi, B. R.; Alzeer, J.; Luedtke, N. W. *ChemBioChem* **2013**, *14*, 540.
(40) (a) Marsich, E.; Piccini, A.; Xodo, L. E.; Manzini, G. *Nucleic Acids Res.* **1996**, *24*, 4029. (b) Marsich, E.; Xodo, L. E.; Manzini, G. *Eur. J. Biochem.* **1998**, *258*, 93.
(41) (a) Oganesian, L.; Karlseder, J. *Mol. Cell* **2011**, *42*, 224. (b) Oganesian, L.; Karlseder, J. *DNA Repair* **2013**, *12*, 238.
(42) Phan, A. T.; Mergny, J. L. *Nucleic Acids Res.* **2002**, *30*, 4618.
(43) Dhakal, S.; Yu, Z. B.; Konik, R.; Cui, Y. X.; Koirala, D.; Mao, H. B. *Biophys. J.* **2012**, *102*, 2575.
(44) Stellwagen, E.; Stellwagen, N. C. *Biophys. J.* **2011**, *100*, Suppl. 1, 58a.
(45) Zhou, J.; Wei, C. Y.; Jia, G. Q.; Wang, X. L.; Feng, Z. C.; Li, C. *Chem. Commun.* **2010**, *46*, 1700.
(46) (a) de Lange, T. *Nat. Rev. Mol. Cell Biol.* **2004**, *5*, 323. (b) Skourti-Stathaki, K.; Proudfoot, N. J. *Genes Dev.* **2014**, *28*, 1384.

DOI: 10.1021/ja508741u
J. Am. Chem. Soc. 2015, 137, 699−707